

framework can effectively accelerate the learning process and accomplish better performance. The contributions of this paper are listed as follows.

- 1) An off-policy actor-critic-based reinforcement learning algorithm is proposed, in which the learning process of the policy network is modified to accordingly combine maximizing the Q-function and imitating the expert demonstration.
- 2) A dynamic experience replay is proposed to adaptively adjust the sampling ratio between the agent's self-exploration and the expert's demonstration in the learning process.
- 3) A comprehensive test is carried out in a simulated challenging urban driving scenario, where various RL and IL baselines are compared against our proposed method.

II. RELATED WORKS

A. Deep reinforcement learning

Much effort has been made and excavated in deep reinforcement learning (DRL), expanding its applications in a wide variety of domains, such as recommending systems, robotic manipulation, and autonomous driving. Previous works have shown that the model-free DRL-based approach is promising for applications in motion control strategies. Zhang *et al.* implemented a vehicle speed control strategy using the double deep Q-network (DDQN), which utilizes visual representation as system input [10]. Chen *et al.* investigated four model-free DRL algorithms for motion control in a roundabout scenario, namely DDPG, TD3, DDQN, and SAC [7], and the results demonstrated that the SAC algorithm outperforms the other methods. DRL has also been applied in specific motion control modules on the vehicle, which delivers favorable and robust performance. Chae *et al.* adopted DQN with a carefully-designed reward function for an adaptive braking system, which could effectively avoid collisions [11]. Ure *et al.* and Chen *et al.* successfully introduced DRL to tune the parameters in MPC [12] and PID [13] controllers, in order to achieve better and more stable performance in path tracking.

B. Imitation learning

Recent developments in the field of deep learning have led to a renewed interest in imitation learning for end-to-end autonomous driving. Dating back to ALVINN [14] decades ago, the behavior cloning method is prevailing in end-to-end autonomous driving, especially recently with the significant improvement brought by deep neural networks. Xu. *et al.* proposed a combination of the fully convolutional network (FCN) and long-short term memory (LSTM) network for learning driving policy [15]. Codevilla *et al.* designed a conditional imitation learning framework which incorporates navigational command inputs [16]. Huang *et al.* presented a multimodal sensor fusion-based end-to-end driving system with imitation learning and scene understanding [17]. More recently, generative adversarial training has been applied in

imitation learning. Inspired by the generative adversarial network (GAN) and its improved versions, Kuefler *et al.* proposed generative adversarial imitation learning (GAIL) for imitating human driving behavior considering the states of multiple surrounding vehicles [18].

C. Combining RL with expert demonstrations

The concept of combining RL with IL for a more efficient learning process has attracted much attention recently. By incorporating small sets of expert demonstration data in pre-training and experience replay, deep Q-learning from demonstrations (DQfD) shows a massively accelerated training process and better performance than the original DQN algorithm [9]. Soft-Q imitation learning (SQIL) [19] provided a similar structure but served as a pure imitation learning approach. Approaches that deal with continuous actions also emerged, such as DDPG from demonstrations (DDPGfD). Their applications in autonomous driving were closely followed. Liu *et al.* [20] utilized DDPG with expert data in track following in The Open Racing Car Simulator (TORCS). Liang *et al.* brought forward controllable imitative reinforcement learning (CIRL) built upon DDPG and imitation learning for urban navigation [21]. Deep imitative model [22] proposed by Rhinehart *et al.* combined R2P2 and imitation learning for improved goal-directed planning. To sum up, the existing approaches that combine RL and IL mostly employ a DDPG-based framework, while the framework based on maximum entropy RL is less-explored.

III. INTEGRATED REINFORCEMENT LEARNING AND IMITATION LEARNING FOR MOTION CONTROL

A. System overview

As shown in Fig. 1, the motion control system is composed of three main parts shown in different colors. The blue part is the driving environment, which receives the actions of the agent and then emits the states of the environment in the form of bird-view images. A route planner generates a goal path that the vehicle should follow, given the start point and destination. Here, we assume that the perception information is perfect, including the states of the ego vehicle and all surrounding objects, and all the information can be projected into a bird-eye view map showing the location of the ego vehicle, the planned route, and surrounding vehicles. The red part is the expert demonstration dataset that we collected in the same environment from a human expert using the steering wheel and pedals. The motion control strategy is explicitly decomposed into two modules, which are longitudinal (acceleration) control with neural network (learnable) and lateral (steering) control with pure-pursuit and PID control (non-learnable) that tracks the predefined route. The learnable module can be trained with any IL or RL algorithms using expert demonstrations or specific rewards, and we train it using the proposed learning framework combining those two together, which is illustrated below.

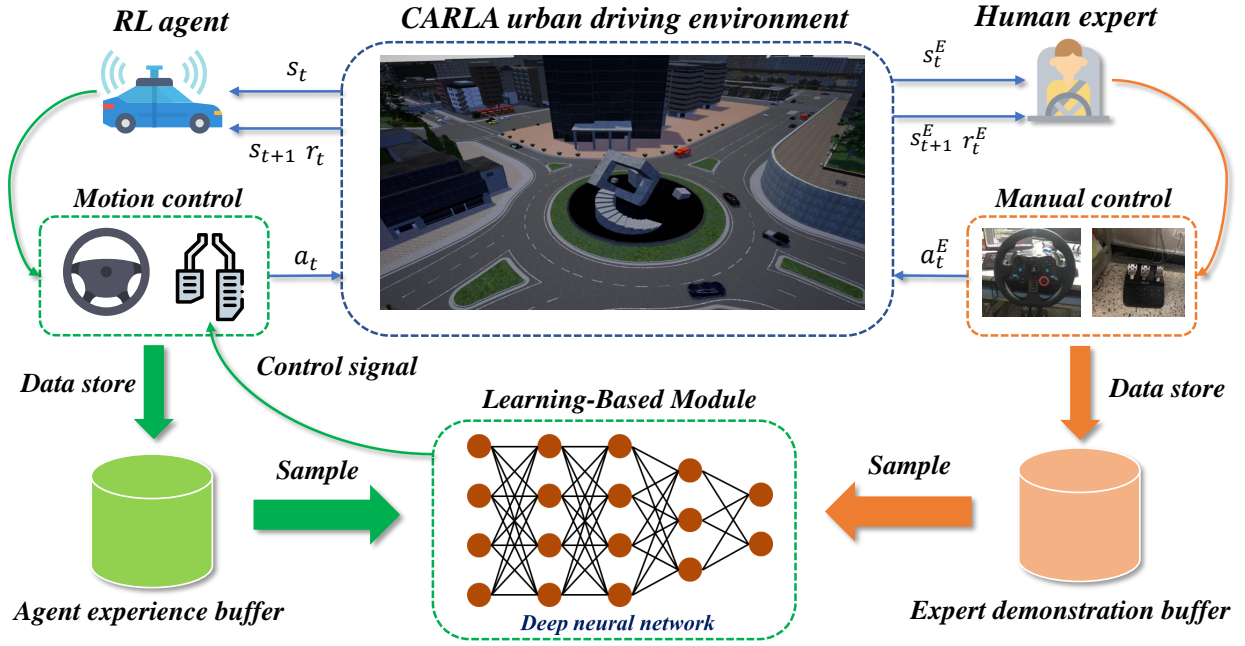


Fig. 1. An overview of our motion control system. The learnable module (deep policy network) receives bird-eye observations and generates throttle command. The lateral motion controller generates the steering command adaptively according to the throttle, predefined route, and vehicle states.

B. Learning framework

The learning process follows the discrete-time Markov decision process (MDP). At every timestep t , the agent receives the state s_t of the environment and executes an action a_t in line with its policy, and the environment returns a reward r_t and transitions to the next state s_{t+1} . The goal of RL is to optimize the policy π_ϕ parameterized by ϕ , so as to maximize the long-term expected returns (Q value): $Q_\pi(s, a) = \mathbb{E}_\pi [\sum_t \gamma^t r(s_t, a_t)]$. On the other hand, imitation learning targets to imitate the expert demonstrations, i.e., reproducing the expert's actions at given states. Assuming that expert demonstrations are gathered in the dataset \mathcal{D}^E in the format of state-action pairs along with the reward and state transition, $\mathcal{D}^E : \left\{ (s_t, a_t, r_t, s_{t+n})^E \right\}_T$, we need to minimize the discrepancy (L2 norm) between the policy's action and the expert's action, mathematically represented by: $\min_\phi \|\pi_\phi(s^E), a^E\|_2$. The core idea of our proposed approach is to add the IL target when using RL to train the motion control strategy, in order to accelerate the training process and hopefully achieve better performance.

To that end, as shown in Fig. 2, we maintain two experience replay buffers to store the agent's self-exploration experiences \mathcal{D}^S and expert demonstrations \mathcal{D}^E separately. The training process has two stages. The initial pre-training stage only involves data from the expert buffer that has been recorded previously. Training the policy network with our proposed IL loss function on the expert demonstration, we get a pre-trained policy network denoted as π_ϕ^E . In the second stage, we initialize the RL training with the pre-trained policy network π_ϕ^E and sample a batch of mixed experiences from those two buffers

with an adaptive ratio at each gradient update step. An off-policy DRL learner (SAC) integrated with imitation learning is introduced to carry out the training and the details of the learning framework are given in the following subsections.

C. Soft actor-critic with imitation learning

We implement the SAC algorithm, augmented by the proposed experience replay mechanism and improved imitation learning loss functions, to train the policy network. SAC optimizes a stochastic policy in an off-policy manner and combines the actor-critic framework with the maximum entropy principle [23], which helps mitigate the issues on exploration-exploitation. The objective of SAC is to maximize a trade-off between expected long-term return and entropy of the policy:

$$\pi^* = \operatorname{argmax}_\pi \mathbb{E}_{\tau \sim \pi} \left[\sum_t \gamma^t (r(s_t, a_t) + \alpha \mathcal{H}(\pi(\cdot|s_t))) \right], \quad (1)$$

where s_t and a_t are the state and action respectively, and α is a non-negative temperature parameter that controls the optimization goal leaning to reward or entropy. The parameter α can be automatically adjusted over the course of training through the following objective:

$$\alpha^* = \operatorname{argmin}_\alpha \mathbb{E}_{a_t \sim \pi} [-\alpha \log \pi(a_t|s_t) - \alpha \bar{\mathcal{H}}], \quad (2)$$

where $\bar{\mathcal{H}}$ is the desired minimum expected entropy.

SAC concurrently learns a policy network π_ϕ , two Q-function networks $Q_{\theta_1}, Q_{\theta_2}$, and a value function network V_ψ . The Q-function networks are updated according to the following loss function:

$$\mathcal{L}(\theta_i)_n = \mathbb{E}_{(s_t, a_t, r, s_{t+n}) \sim \mathcal{D}} \left[(Q_{\theta_i}(s_t, a_t) - y_Q)^2 \right], \quad (3)$$

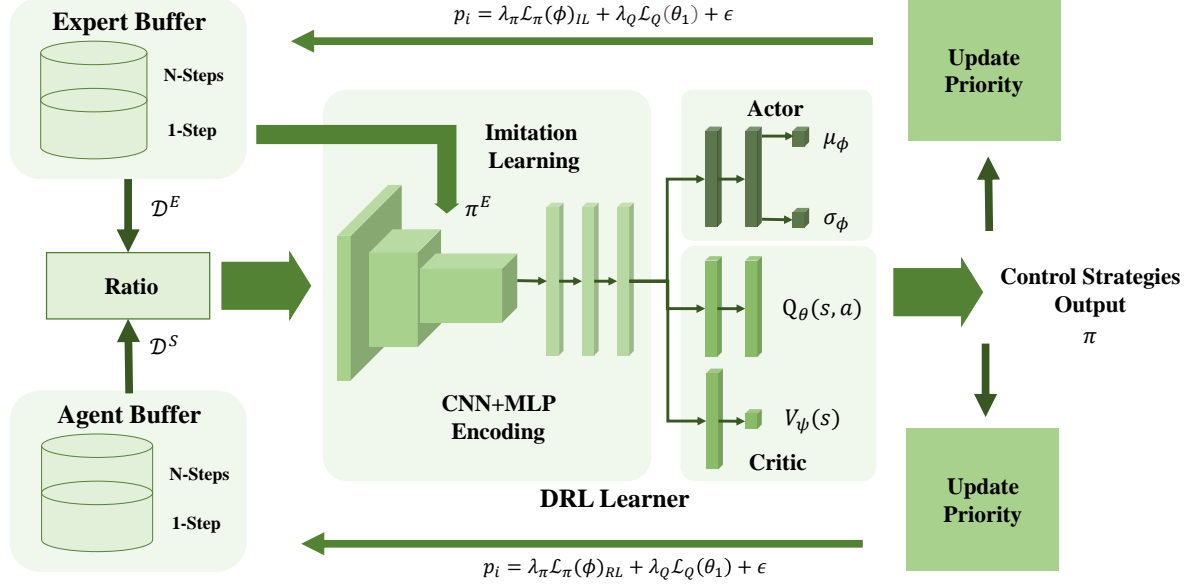


Fig. 2. The diagram of the proposed learning framework combining RL and IL. Training process consists of IL pre-training and DRL training. Batched tuple data from agent and expert is sampled from two adaptive prioritized replay buffers, which contain mapped 1-step and N-steps transitions.

where $i = 1, 2$, n stands for n-step Q-learning, \mathcal{D} is composed of the experience collected by both the agent's self-exploration and the expert's demonstration $\mathcal{D} = \mathcal{D}^E \cup \mathcal{D}^S$, and y_Q is the target. Using n-step loss enables the agent to consider a series of transitions to look further into the future and prevent the policy from a bad local optimum. The n-step return is defined as:

$$r(s_t, a_t, n) = \sum_{k=0}^{n-1} \gamma^k r(s_{t+k}, a_{t+k}). \quad (4)$$

Therefore, the target for Q-function update is given by:

$$y_Q = r(s_t, a_t, n) + \gamma^n V_{\text{target}}(s_{t+n}), \quad (5)$$

where V_{target} is the target value function network, which is obtained by polyak averaging the value network V_ψ parameters at each gradient step. We use a mix of 1-step and n-step losses when updating the Q-function networks, i.e., $\mathcal{L}(\theta_i) = \mathcal{L}(\theta_i)_1 + \mathcal{L}(\theta_i)_n$.

The value function network V_ψ gets update through the following loss function:

$$\mathcal{L}(\psi) = \mathbb{E}_{s_t \sim \mathcal{D}} \left[(V_\psi(s_t) - y_V)^2 \right], \quad (6)$$

and the target for value function is given by:

$$y_V = \min_{i=1,2} Q_{\theta_i}(s_t, \tilde{a}_t) - \alpha \log \pi_\phi(\tilde{a}_t | s_t), \quad (7)$$

where the actions are sampled fresh from the policy $\tilde{a}_t \sim \pi_\phi(\cdot | s_t)$, whereas the states should come from the replay buffer $s_t \sim \mathcal{D}$.

For the policy network, it can be trained with both imitation learning and reinforcement learning leveraging the experiences from the expert demonstration and the agent's exploration, respectively. For reinforcement learning, the policy network should be updated to maximize the expected future return plus expected future entropy. Making use of the reparameterization trick, in which a sample from the stochastic policy $\pi_\phi(\cdot | s_t)$ is drawn by computing the following deterministic function:

$$\tilde{a}_\phi(s_t, \xi) = \tanh(\mu_\phi(s_t) + \sigma_\phi(s_t) \odot \xi), \quad \xi \sim \mathcal{N}(0, I),$$

the loss function for the policy network π_ϕ when learning from the agent's experience should be:

$$\mathcal{L}(\phi)_{RL} = \mathbb{E}_{s_t \sim \mathcal{D}^S, \xi \sim \mathcal{N}} \left[\alpha \log \pi_\phi(\tilde{a}_\phi(s_t, \xi) | s_t) - \min_{i=1,2} Q_{\theta_i}(s_t, \tilde{a}_\phi(s_t, \xi)) \right]. \quad (8)$$

For learning from expert demonstrations or imitation learning, the loss function for updating the policy network π_ϕ becomes:

$$\mathcal{L}(\phi)_{IL} = \mathbb{E}_{(s_t, a_t) \sim \mathcal{D}^E} \left[(\tilde{a}_\phi(s_t) - a_t)^2 \right], \quad (9)$$

where \mathcal{D}^E is the buffer that contains expert demonstrations.

In the imitation loss function Eq. (9), the agent's action $\tilde{a}_\phi(s_t)$ is the mean value of the stochastic policy $\tanh(\mu_\phi(s_t))$, instead of a sample from the action distribution. In addition, we add a Q-value regularization so as to combat the overfitting issue and boost the learning speed, which means

the imitation loss is only referred to if the following condition is satisfied:

$$Q_{\theta_j}(s_t^E, a_t^E) \geq \min_{i=1,2} Q_{\theta_i}(s_t^E, a_\phi(s_t^E)), \quad (10)$$

where $j = 1, 2$, meaning any of the two Q-function networks can trigger the condition.

Eq. (10) illustrates that the policy network will cease imitation loss update when the agent’s performance (Q-value) outweighs the expert. Empirically speaking, adding this constraint can effectively adjust the imitation learning process and filter the suboptimal demonstrations, and avoid overfitting the policy to expert demonstrations.

Putting it all together, the loss function for the policy network π_ϕ in SAC with imitation learning is:

$$\mathcal{L}(\phi) = \begin{cases} \alpha \log \pi_\phi(\tilde{a}_\phi(s_t, \xi) | s_t) - \min_{i=1,2} Q_{\theta_i}(s_t, \tilde{a}_\phi(s_t, \xi)) & \text{if } s_t \sim \mathcal{D}^S, \\ (\tilde{a}_\phi(s_t) - a_t)^2 & \text{if } (s_t, a_t) \sim \mathcal{D}^E \text{ and Eq. (10)}. \end{cases} \quad (11)$$

In the initial offline per-training stage, the policy network gets trained using behavior cloning with the recorded expert demonstrations (state-action pairs). This helps the actor’s performance quickly amount to the level of expert, which could significantly accelerate the training process. In the subsequent online training stage, to balance the sources of experience the agent learns from (i.e., the ratio of the agent’s experience and expert’s demonstration), we design a mechanism of experience replay that can adaptively sample experiences from the two sources, which is explained below.

D. Adaptive prioritized experience replay

Following the prioritized experience replay (PER) mechanism [24], each transition tuple in the two replay buffers will be assigned a priority, such that more important transition tuples with greater approximation errors can more likely be sampled. This way, the sampling process becomes more efficient and goal-directed, which is essential to deal with the problems with sparse reward. The devised priority p_i for transition tuple i in the agent replay buffer is

$$p_i = \lambda_\pi \mathcal{L}_\pi(\phi)_{RL} + \lambda_Q \mathcal{L}_Q(\theta_1) + \epsilon, \quad (12)$$

where λ_π and λ_Q are the weights to balance the importance of each error term, and ϵ is a small positive constant to ensure that all transitions are sampled with some non-zero probability. Likewise, the priority p_i for transition tuple i in the expert replay buffer is

$$p_i = \lambda_\pi \mathcal{L}_\pi(\phi)_{IL} + \lambda_Q \mathcal{L}_Q(\theta_1) + \epsilon. \quad (13)$$

The probability for a transition tuple being sampled is $P(i) = \frac{p_i^\alpha}{\sum_k p_k^\alpha}$, in which α is a hyper-parameter that determines the level of prioritization. To correct the bias introduced by not uniformly sampling during backpropagation, an importance-sampling weight is assigned to the loss regarding the transition tuple $\omega(i) = (\frac{1}{NP(i)})^\beta$, where N is the number

of experiences and β is another hyper-parameter that controls how much prioritization to apply.

We sample the experiences separately for expert and agent buffers for RL training while updating the priorities of them, and the ratio of the samples from the two sources is dynamically adjusted using the following equation:

$$\mathcal{B} \leftarrow (\rho \mathcal{B} \sim \mathcal{D}^S) \cup ((1 - \rho) \mathcal{B} \sim \mathcal{D}^E), \quad (14)$$

where \mathcal{B} is the mini-batch, and $\rho \in [0.75, 1]$ is the sampling ratio, calculated as:

$$\rho \leftarrow \rho + \frac{2}{N} \mathbb{1} \left(\sum_t r_t^A \geq \bar{r}^E \right), \quad (15)$$

where $N_{\mathcal{B}}$ is the current size of the mini-batch, r_t^A denotes the agent’s step reward, and \bar{r}^E represents the average episodic reward of the expert demonstration.

Eq. (15) indicates a dynamic update rule that the sampling ratio for the agent buffer will gradually increase if the episodic reward for the agent is greater than the average performance of the expert.

IV. EXPERIMENTS

A. Experimental Setup

We employ the CARLA simulator [25] as the experimental platform, since it possesses abundant vehicle models and maps close to the real world, thus being suitable for urban driving simulation. In the experiment, the vehicle needs to run safely and efficiently through a roundabout consisting of multiple intersections in the urban area, shown in Fig. 3(a). An agent vehicle is first spawned randomly in the starting area and follows the planned route to the destination, while avoiding collisions with the surrounding vehicles in the dense traffic. A total of N_{vehicle} surrounding vehicles are randomly spawned in the scene, each is assigned with a random route in one training episode, and they can perform emergency stop when encountering red light or vehicles.

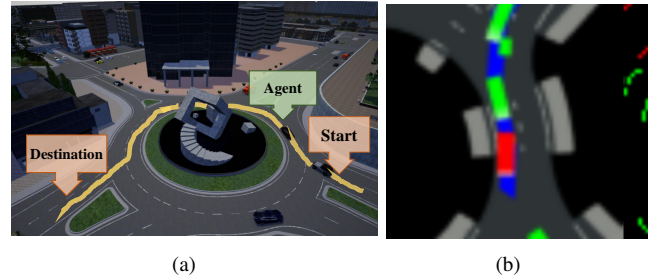


Fig. 3. Overview of the urban driving task and processed scene representation: (a) overview of the roundabout; (b) an example of bird-view image input.

We take the bird-eye view image shown in Fig. 3(b) as the scene representation because it contains rich information of the agent vehicle and its route, the road topology, and surrounding vehicles. The historical positions of the ego vehicle are also shown in the bird-eye view image to incorporate the information from the time domain. The image is with

a size of $64 \times 64 \times 3$ and collected every time step dt . The continuous action space is the normalized throttle and brake control $[-1, 1]$, where $[-1, 0]$ is for brake input and $[0, 1]$ for throttle input, while the discrete action space consists of three actions corresponding to the normalized throttle and brake, which are $\{-1, 0, 1\}$. The lateral control (steering) is governed by a combination of a PID controller and a pure-pursuit controller to track the target waypoint. In the data collection stage, we record a human expert's continuous data on pedal control via a Logitech G29 racing set, and discrete maneuvers by pressing the keyboard. Overall, a total of 50 trajectories of expert demonstrations are collected, with approximately 15,000 transition tuples.

The policy network utilizes the convolutional neural network (CNN) structure as the feature extractor and generates the mean and standard deviation of a Gaussian distribution through two fully connected layers each with 64 hidden units. The critic networks' feature extractors share the same CNN structure.

B. Reward function

Considering that safety is the most critical in autonomous driving, we design a reward function that focuses on safety factor while keeping a balance on efficiency and ride comfort. After some trials, the reward function is devised as a combination of four features:

$$r_t = r_v + r_{step} + r_{col} + r_{safe}. \quad (16)$$

The first term r_v is for travel efficiency, which stimulates the agent to run as fast as possible but within the speed limit v_{max} :

$$r_v = v + 2(v_{max} - v) \mathbb{1}(v \geq v_{max}), \quad (17)$$

where v is the speed of the ego vehicle.

The second term r_{step} is a small constant penalty (-0.1) also devised for travel efficiency, which is to encourage the agent to complete the task as quickly as possible.

The other two terms are set for ensuring safety. First of all, r_{col} is a penalty for collision, as large as -10 if any collision happens. However, such supervision could be too weak and lead to spurious correlations between some irrelevant features and actions. Therefore, to provide more information into the reward signal, we consider the potential danger in a front-detection area shown in Fig. 4. It consists of two fan-shape areas $Z_1(\alpha_1, r_1)$ and $Z_2(\alpha_2, r_2)$, where α_i is the detect angle and r_i is the radius. Z_2 is a long-range detection area originating from the vehicle center (x_A, y_A) for tasks such as car following. Z_1 , centered at $(x_A + \frac{L_{wb}}{2}, y_A)$ where L_{wb} is the length of the wheelbase, is responsible for short distance sensing like a car passing by in front of ego vehicle. If multiple vehicles are in an area Z_i , only the nearest vehicle is detected and its distance to a certain center point d_i will be returned. Utilizing the information above, we can derive the safety reward r_{safe} :

$$r_{safe} = - \left[\lambda_s \frac{r_1 - d_1}{r_1} \mathbb{1}(d_1) + (1 - \lambda_s) \frac{r_2 - d_2}{r_2} \mathbb{1}(d_2) \right] v_{safe} \quad (18)$$

where λ_s is a weight balancing the importance of the two areas, d_i is the distance of the ego vehicle to the nearest vehicle in each area Z_i , and v_{safe} is a speed-related regulator:

$$v_{safe} = (1 + v) [1 - \mathbb{1}(v \leq v_{min}, a_t \leq 0)], \quad (19)$$

where v_{min} is a speed threshold and a_t is the agent's action.

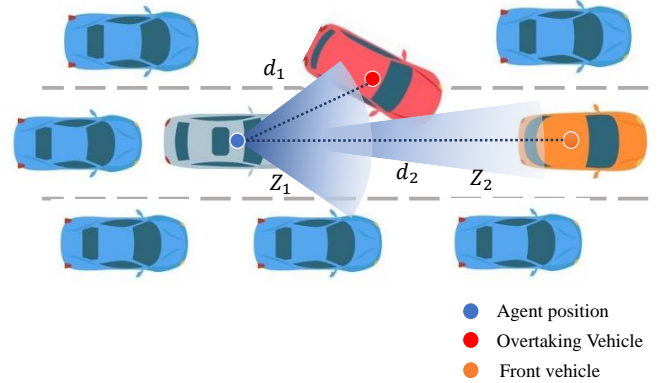


Fig. 4. Illustration of the front-detection area for the ego vehicle.

Eq. (18) directs the ego vehicle to avoid collisions, since the normalized term will be close to 1 if two vehicles are too close, and thus the penalty will increase. If there is no vehicle in the detection zone, the normalized term will be 0 due to the indicator term, and no penalty is given. We also add a regulator (Eq. (19)) to the safety penalty, which increases the penalty if the ego vehicle is running fast when there is a potential danger in the front zone and removes the penalty if the ego vehicle decelerates or waits when facing traffic congestion.

C. Comparison baselines

To make a comprehensive evaluation of the performance of the proposed approach, we compare it with other existing methods from the field of deep reinforcement learning, imitation learning, and reinforcement learning from demonstrations. The baseline DRL algorithms are:

- 1) **DQN** [26]: one of the first and most-commonly known DRL methods. It is a value-based method and Q-function loss gets update through one-step temporal difference error.
- 2) **PPO** [27]: an on-policy method and has been widely used in robotics control.
- 3) **TD3** [28]: an improved method with twin delayed Q-networks based on the DDPG algorithm.
- 4) **A3C** [29]: an on-policy actor-critic framework with asynchronous sampling and advantage estimation.
- 5) **SAC** [23]: the basis of our approach, which has been recently reported with higher performance in practical applications.

The imitation learning baseline methods are listed as follows:

- 1) **BC**: behavioral cloning is a supervised learning method, which has been commonly used in learning driving policy from expert demonstrations.

2) **SQL** [19]: a regularized behavioral cloning method, which combines the maximum likelihood of BC with regularization that can stimulate the agent return to demonstrated states upon encountering new states.

3) **GAIL** [30]: a variant of imitation learning using generative adversarial training, in which the generator is RL-based and the reward function comes from the discriminator that tries to tell apart the demonstrated and generated trajectories.

D. Implementation details

In the pre-training stage, the policy network gets pre-trained with the imitation learning loss for 10k steps using the expert demonstration dataset. In the online training stage, our proposed approach and other baseline methods are trained for 100k steps. The neural networks are trained on a single NVIDIA RTX 2070 Super GPU using Tensorflow and Adam optimizer with a learning rate of 3×10^{-4} , and the online training process takes roughly 6 hours. The parameters related to the experiment are listed in Table I.

TABLE I
PARAMETERS USED IN THE EXPERIMENT

Notation	Meaning	Value
N_{vehicle}	Number of surrounding vehicles	150
dt	Time step (s)	0.1
v_{max}	Speed limit (m/s)	8
v_{min}	Speed threshold (m/s)	0.1
$\alpha_{i=1,2}$	Angles of front detection area (deg)	60, 30
$r_{i=1,2}$	Radius of front detection area (m)	10, 18
λ_s	Safety balance weight	0.8
L_{wb}	Wheelbase (mm)	2850
γ	Discount rate	0.995
\mathcal{H}	Desired minimum expected entropy	-1
n	N-step Q-learning	10
N_{buffer}^r	Agent buffer capacity	50000
$N_{\mathcal{B}}$	Mini-batch size	64
α	Hyperparameter for PER	0.6
β	Hyperparameter for PER	$0.4 \rightarrow 1$
ϵ	Hyperparameter for PER	10^{-6}
λ_π	Priority balance weight	1
λ_Q	Priority balance weight	1

V. RESULTS AND DISCUSSIONS

A. Training results

We evaluate the training performance of our proposed method in comparison with other RL and IL methods introduced in the previous section. In Fig. 5, we take the best training result of each baseline algorithm for 100k training steps, the black dotted line represents an average episode reward (940.81) that an agent can get reaching the destination area, and the grey shade in Fig. 6 is the performance of our collected expert demonstrations with an average of 1060.4 and standard deviation of 227.0.

As seen in Fig. 5, our approach shows the highest average episodic reward and is basically above the average reward line to reach the destination. It starts with a relatively high reward because of the pretraining phase with imitation learning. At the beginning of the training process, with a larger ratio of samples

from expert demonstration, the agent is basically imitating the expert demonstration with high rewards. Then, our proposed adaptive prioritized replay will gradually lower the ratio to sample more experience from the agent’s self-exploration, and thus the training process naturally transits to the reinforcement learning.

Compared with other RL baseline methods, our proposed method shows a faster convergence speed and better performance at the end. We can find out that the average episodic reward of the proposed method quickly climbs to a very high level and gradually improves and finally converges after roughly 40k step. For the other methods, A3C behaves significantly poor and is unable to even reach the entrance of the roundabout. It is because the traffic scenario for each training epoch is notably different, and the A3C policy easily falls into a local minimum of staying close to the starting point. PPO can skip the local optimal problem and learns efficiently, but cannot learn to reach the destination with dense traffic. The three off-policy algorithms can basically reach the destination. SAC performs the best but takes longer steps to converge. DQN actually performs well in this case by adding double Q-networks, dueling branch, and PER. This is because the value-based method can at least guarantee the training progress, but is heavily relied on the design of the reward function. TD3 takes the longest steps to actually improve the policy, and is very unstable in performance during our experiment: it shows no progress without adding noise, but after adding the noise, its performance still varies greatly.

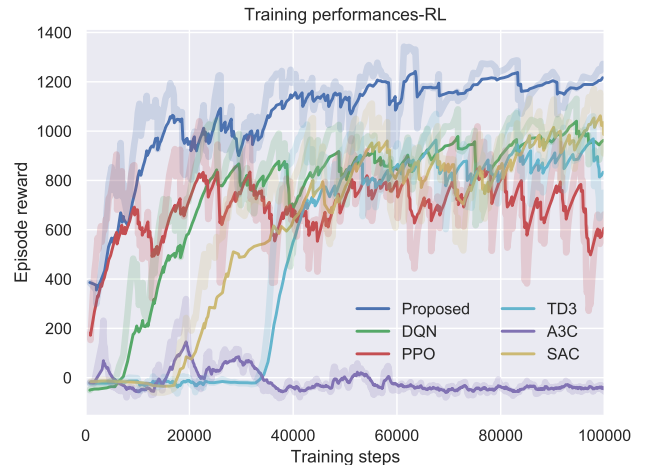


Fig. 5. The training curves of RL baselines and our approach. Our approach shows the highest episode reward than other methods.

In comparison with other IL baseline methods, our approach converges quite fast and reaches the level of the human expert. SQL can also converge very fast but performs notably worse in terms of average episodic reward than our method as it only uses expert demonstration data. GAIL shows the worst performance even with 10k steps of pretraining, probably due to its insensitive response to image input, which has also been mentioned by [8] and [19]. The results show that our

approach not only imitates the expert demonstrations but also improves its behavior to some extent because of adding RL to the framework.



Fig. 6. The training curves of IL baselines and our approach. Our approach shows a faster convergence as well as steady progress.

B. Testing results

The summary of test performance of all the methods is given in Table II. Each method is tested 100 times in the roundabout with different traffic participants, and the success rate, as well as the average episodic reward and steps are recorded. The results reflect that our proposed approach shows a high success rate, as well as reaching the destination in a shorter time. As discussed above, A3C does not perform well, and the vanilla BC method also suffers from a low success rate due to the distributional shift during the test. SAC and DQN show good performance during the test, and SQIL is also quite effective in solving this problem.

TABLE II
SUMMARY OF THE TEST RESULTS

Approach	Success rate (%)	Episode reward	Episode length
DQN	79	1006.3 ± 191.28	384 ± 84
PPO	65	903.69 ± 253.74	321 ± 83
TD3	67	802.45 ± 184.66	316 ± 59
A3C	18	39.844 ± 42.764	493 ± 25
SAC	76	1050.9 ± 205.80	410 ± 84
BC	16	987.37 ± 248.60	487 ± 104
GAIL	65	769.32 ± 235.47	245 ± 64
SQIL	78	966.35 ± 199.13	382 ± 82
Ours	90	1205.3 ± 135.79	239 ± 65

Here, we give some qualitative results by showing some of the trajectories given by our proposed motion control strategy in Fig. 7, where the ego vehicle is able to cruise at a safe distance following the front vehicle. The agent can go through the roundabout scene with smooth turnings and decelerate gradually when facing stopped cars in the front. Most of the trajectories come to an end in the destination area, which

means the agent has successfully finished the task. However, the faint yellow points indicate the failure cases, which are mostly owing to collisions with the front vehicle or overtaking vehicles from the side. The collisions that happened right into the roundabout mainly come from the vehicles from the left or right side since the blind angle for the detection area gets larger when going into the roundabout. There are some failure cases at the very beginning because of the control failure of the surrounding vehicles, which cause a collision with the ego vehicle.



Fig. 7. An overview of vehicle trajectories of the proposed method during the test. The orange areas represent the starting and destination zones. The yellow points show where the trajectory ends.

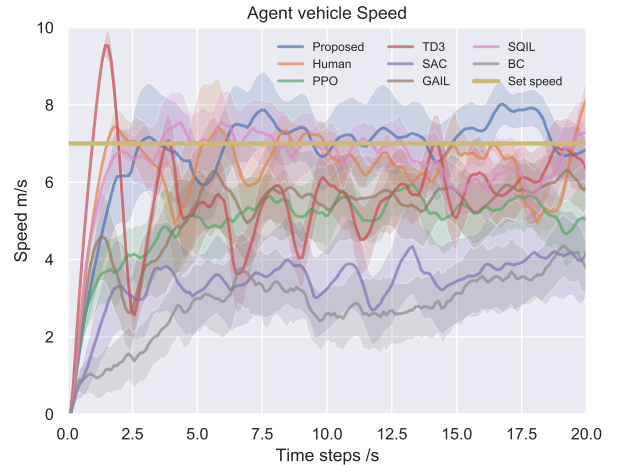


Fig. 8. The average speed and its standard deviation for each method of the first 20 seconds after the initial acceleration

To have a more intuitive sense of the safety and efficiency issues, we had a further look at the speed performance of each method. In addition to the aforementioned approach, we

also randomly sampled 30 human trajectories in the expert dataset. Speed information of the first 20 seconds from the beginning of initial acceleration is calculated for each method. As shown in Fig. 8, when the target speed is set to 7 m/s, our proposed method can respond immediately and reach the target speed in roughly 2 seconds, which is very close to the performance of a human expert. SQIL method can also deliver close-to-human performance. TD3 method reacts the fastest, but its speed varies greatly after the initial acceleration, which obviously cannot guarantee safety. Other RL agents accelerate steadily but are unable to reach the target speed in 20 seconds.

VI. CONCLUSIONS

In this paper, we propose a motion control strategy for urban autonomous driving, with an improved design that incorporates deep reinforcement learning with expert demonstrations. A novel reinforcement learning algorithm is put forward to leverage expert demonstrations, so as to improve the sample efficiency and performance. Specifically, we modify the update of the policy network by combining maximizing the Q-function and imitating the expert's actions, and design an adaptive experience replay method to adaptively sample experience from the agent's self-exploration and expert demonstration for policy update. We validate the proposed method in a simulated challenging urban roundabout scenario with dense traffic. A comprehensive comparison with other RL and IL baselines proves that our method has better sample efficiency and performance in the training process. The testing result reveals that our proposed method achieves a higher success rate with less time to reach the destination, showing promising potential for our approach applied in the autonomous vehicle's motion control strategy.

REFERENCES

- [1] J. Levinson, J. Askeland, J. Becker, J. Dolson, D. Held, S. Kammel, J. Z. Kolter, D. Langer, O. Pink, V. Pratt, M. Sokolsky, G. Stanek, D. Stavens, A. Teichman, M. Werling, and S. Thrun, "Towards fully autonomous driving: Systems and algorithms," in *2011 IEEE Intelligent Vehicles Symposium (IV)*, 2011, pp. 163–168.
- [2] S. Mozaffari, O. Y. Al-Jarrah, M. Dianati, P. Jennings, and A. Mouzakis, "Deep learning-based vehicle behavior prediction for autonomous driving applications: A review," *IEEE Transactions on Intelligent Transportation Systems*, 2020.
- [3] E. van Nunen, M. R. Kwakernaat, J. Ploeg, and B. D. Netten, "Cooperative competition for future mobility," *IEEE Transactions on Intelligent Transportation Systems*, vol. 13, no. 3, pp. 1018–1025, 2012.
- [4] L. Chen *et al.*, "A reinforcement learning-based adaptive path tracking approach for autonomous driving," *IEEE Transactions on Vehicular Technology*, 2020.
- [5] S. Panwai and H. Dia, "Comparative evaluation of microscopic car-following behavior," *IEEE Transactions on Intelligent Transportation Systems*, vol. 6, no. 3, pp. 314–325, 2005.
- [6] A. O. Ly and M. A. Akhloufi, "Learning to drive by imitation: an overview of deep behavior cloning methods," *IEEE Transactions on Intelligent Vehicles*, 2020.
- [7] J. Chen, B. Yuan, and M. Tomizuka, "Model-free deep reinforcement learning for urban autonomous driving," in *2019 IEEE Intelligent Transportation Systems Conference (ITSC)*. IEEE, 2019, pp. 2765–2771.
- [8] K. Brantley, W. Sun, and M. Henaff, "Disagreement-regularized imitation learning," in *International Conference on Learning Representations*, 2019.
- [9] T. Hester, M. Vecerik, O. Pietquin, M. Lanctot, T. Schaul, B. Piot, D. Horgan, J. Quan, A. Sendonaris, G. Dulac-Arnold *et al.*, "Deep q-learning from demonstrations," *arXiv preprint arXiv:1704.03732*, 2017.
- [10] Y. Zhang, P. Sun, Y. Yin, L. Lin, and X. Wang, "Human-like autonomous vehicle speed control by deep reinforcement learning with double q-learning," in *2018 IEEE Intelligent Vehicles Symposium (IV)*. IEEE, 2018, pp. 1251–1256.
- [11] H. Chae, C. M. Kang, B. Kim, J. Kim, C. C. Chung, and J. W. Choi, "Autonomous braking system via deep reinforcement learning," in *2017 IEEE 20th International Conference on Intelligent Transportation Systems (ITSC)*. IEEE, 2017, pp. 1–6.
- [12] N. K. Ure, M. U. Yavas, A. Alizadeh, and C. Kurtulus, "Enhancing situational awareness and performance of adaptive cruise control through model predictive control and deep reinforcement learning," in *2019 IEEE Intelligent Vehicles Symposium (IV)*. IEEE, 2019, pp. 626–631.
- [13] L. Chen, Y. Chen, X. Yao, Y. Shan, and L. Chen, "An adaptive path tracking controller based on reinforcement learning with urban driving application," in *2019 IEEE Intelligent Vehicles Symposium (IV)*. IEEE, 2019, pp. 2411–2416.
- [14] D. A. Pomerleau, "Alvinn: An autonomous land vehicle in a neural network," in *Advances in neural information processing systems*, 1989, pp. 305–313.
- [15] H. Xu, Y. Gao, F. Yu, and T. Darrell, "End-to-end learning of driving models from large-scale video datasets," in *Proceedings of the IEEE conference on computer vision and pattern recognition*, 2017, pp. 2174–2182.
- [16] F. Codevilla, M. Müller, A. López, V. Koltun, and A. Dosovitskiy, "End-to-end driving via conditional imitation learning," in *2018 IEEE International Conference on Robotics and Automation (ICRA)*. IEEE, 2018, pp. 1–9.
- [17] Z. Huang, C. Lv, Y. Xing, and J. Wu, "Multi-modal sensor fusion-based deep neural network for end-to-end autonomous driving with scene understanding," *IEEE Sensors Journal*, pp. 1–1, 2020.
- [18] A. Kuefler, J. Morton, T. Wheeler, and M. Kochenderfer, "Imitating driver behavior with generative adversarial networks," in *2017 IEEE Intelligent Vehicles Symposium (IV)*. IEEE, 2017, pp. 204–211.
- [19] S. Reddy, A. D. Dragan, and S. Levine, "Sqil: Imitation learning via reinforcement learning with sparse rewards," *arXiv preprint arXiv:1905.11108*, 2019.
- [20] K. Liu, Q. Wan, and Y. Li, "A deep reinforcement learning algorithm with expert demonstrations and supervised loss and its application in autonomous driving," in *2018 37th Chinese Control Conference (CCC)*. IEEE, 2018, pp. 2944–2949.
- [21] X. Liang, T. Wang, L. Yang, and E. Xing, "Cirl: Controllable imitative reinforcement learning for vision-based self-driving," in *Proceedings of the European Conference on Computer Vision (ECCV)*, 2018, pp. 584–599.
- [22] N. Rhinehart, R. McAllister, and S. Levine, "Deep imitative models for flexible inference, planning, and control," *arXiv preprint arXiv:1810.06544*, 2018.
- [23] T. Haarnoja, A. Zhou, P. Abbeel, and S. Levine, "Soft actor-critic: Off-policy maximum entropy deep reinforcement learning with a stochastic actor," *arXiv preprint arXiv:1801.01290*, 2018.
- [24] T. Schaul, J. Quan, I. Antonoglou, and D. Silver, "Prioritized experience replay," *arXiv preprint arXiv:1511.05952*, 2015.
- [25] A. Dosovitskiy, G. Ros, F. Codevilla, A. Lopez, and V. Koltun, "Carla: An open urban driving simulator," *arXiv preprint arXiv:1711.03938*, 2017.
- [26] H. Van Hasselt, A. Guez, and D. Silver, "Deep reinforcement learning with double q-learning," *arXiv preprint arXiv:1509.06461*, 2015.
- [27] J. Schulman, F. Wolski, P. Dhariwal, A. Radford, and O. Klimov, "Proximal policy optimization algorithms," *arXiv preprint arXiv:1707.06347*, 2017.
- [28] S. Fujimoto, H. Van Hoof, and D. Meger, "Addressing function approximation error in actor-critic methods," *arXiv preprint arXiv:1802.09477*, 2018.
- [29] V. Mnih, A. P. Badia, M. Mirza, A. Graves, T. Lillicrap, T. Harley, D. Silver, and K. Kavukcuoglu, "Asynchronous methods for deep reinforcement learning," in *International conference on machine learning*, 2016, pp. 1928–1937.
- [30] J. Ho and S. Ermon, "Generative adversarial imitation learning," in *Advances in neural information processing systems*, 2016, pp. 4565–4573.